# Configurations of the Re-scan Confocal Microscope (RCM) for biomedical applications

De Luca, G.M.R.; Desclos, E.; Breedijk, R.M.P.; Dolz-Edo, L.; Smits, G.J.; Nahidiazar, L.; Bielefeld, P.; Picavet, L.; Fitzsimons, C.P.; Hoebe, R.; Manders, E.M.M.

**DOI**
10.1111/jmi.12526

**Publication date**
2017

**Document Version**
Final published version

**Published in**
Journal of Microscopy

Journal of Microscopy

*Journal of Microscopy, Vol. 266, Issue 2 2017, pp. 166–177* doi: 10.1111/jmi.12526
*Received 21 April 2016; accepted 4 January 2017*

# Configurations of the Re-scan Confocal Microscope (RCM) for biomedical applications

G.M.R. DE LUCA*, E. DESCLOS*, R.M.P. BREEDIJK*, L. DOLZ-EDO†, G.J. SMITS†, L. NAHIDIAZAR‡, P. BIELEFELD§, L. PICAVET§, C.P. FITZSIMONS§, R. HOEBE‖ & E.M.M. MANDERS*,#

*Van Leeuwenhoek Centre for Advanced Microscopy, Swammerdam Institute for Life Sciences, University of Amsterdam, Amsterdam, The Netherlands
†Molecular Biology and Microbial Food Safety, Swammerdam Institute for Life Sciences, University of Amsterdam, Amsterdam, The Netherlands
‡Division of Cell Biology, The Netherlands Cancer Institute, Plesmanlaan 121, Amsterdam 1066 CX, The Netherlands
§Center for Neuroscience, Swammerdam Institute for Life Sciences, University of Amsterdam, The Netherlands
‖Van Leeuwenhoek Centre for Advanced Microscopy, Department of Cell Biology and Histology, Academic Medical Centre, Amsterdam, The Netherlands
#Nikon Centre of Excellence on Super Resolution Microscopy Development, University of Amsterdam, Amsterdam, The Netherlands

**Key words.** High-sensitive microscopy, live cell imaging, multicolour microscopy, super-resolution microscopy.

## Summary

The new high-sensitive and high-resolution technique, Re-scan Confocal Microscopy (RCM), is based on a standard confocal microscope extended with a re-scan detection unit. The re-scan unit includes a pair of re-scanning mirrors that project the emission light onto a camera in a scanning manner. The signal-to-noise ratio of Re-scan Confocal Microscopy is improved by a factor of 4 compared to standard confocal microscopy and the lateral resolution of Re-scan Confocal Microscopy is 170 nm (compared to 240 nm for diffraction limited resolution, 488 nm excitation, 1.49 NA). Apart from improved sensitivity and resolution, the optical setup of Re-scan Confocal Microscopy is flexible in its configuration in terms of control of the mirrors, lasers and filters. Because of this flexibility, the Re-scan Confocal Microscopy can be configured to address specific biological applications. In this paper, we explore a number of possible configurations of Re-scan Confocal Microscopy for specific biomedical applications such as multicolour, FRET, ratio-metric (e.g. pH and intracellular $Ca^{2+}$ measurements) and FRAP imaging.

## Introduction

In the last decades, fluorescence microscopy has grown in research potential by the strong improvement of the optical resolution and by the possibility to observe dynamic behaviour of molecules in living cells with functional imaging. High-resolution and high-sensitive imaging combined with multicolour imaging and functional imaging have proven to be essential for the analysis of specific biological processes (Schermelleh *et al.*, 2010). Super-resolution techniques like Structured Illumination Microscopy (SIM), Stimulated emission depletion (STED), Stochastic optical reconstruction microscopy (STORM) and Photo-activated localization microscopy (PALM) have enabled fluorescence imaging with improved spatial resolution (Betzig *et al.*, 2006; Hess *et al.*, 2006; Rust *et al.*, 2006; Leung & Keng, 2011). Although these new techniques are growing in popularity in the scientific community, they still show some drawbacks in multicolour and fast acquisition in living cells (Marx, 2013) and for this reason wide-field fluorescence microscopy and confocal microscopy are still widely used for a variety of biological studies. In this paper, we will show how Re-scan Confocal Microscopy (RCM), a confocal technique with improved resolution and sensitivity, can be used in several morphological and functional applications.

RCM is a new optics-only super-resolution technique based on standard confocal microscopy (De Luca *et al.*, 2013; De Luca, submitted). The RCM setup is based on a standard confocal microscope extended with a re-scan detection unit. The re-scan unit includes a pair of re-scanning mirrors that direct the emission light onto a sensitive sCMOS camera in a scanning manner. RCM has been shown (De Luca, submitted) to provide 170 nm lateral resolution (at 488 nm excitation). This resolution is independent from the pinhole diameter (De Luca *et al.*, 2013; De Luca, submitted) in contrast with standard confocal microscopy where the higher resolution is only possible with almost closed pinhole (<< 1 A.U. (Airy Units)). For similar lateral resolution, obtained with RCM with a pinhole

[Correction added on 6 April 2017, after first online publication: Author "L. Nahidiazar", originally omitted, has been added to the author list]

Correspondence to: Giulia M.R. De Luca, Van Leeuwenhoek Centre for Advanced Microscopy, Swammerdam Institute for Life Sciences, University of Amsterdam, Amsterdam, The Netherlands. e-mail: g.deluca@uva.nl

diameter of 2 A.U. and with standard confocal microscopy equipped with PhotoMultiplier Tube (PMT)s with 0.5 A.U. pinhole diameter, RCM offers four times improved signal-to-noise ratio because of the combination of open pinhole and sensitive camera detection (De Luca, submitted).

RCM is a fully optical implementation of an idea described by Sheppard in 1988 (Sheppard, 1988) where he demonstrated that the lateral resolution of the confocal microscopy can be improved by using the spatial information of the distribution of light at the pinhole plane. This idea was implemented for the first time in image scanning microscopy (Muller & Enderlein, 2010) where several images are recorded, forming a final single high-resolution image by a postprocessing image reconstruction procedure. In the last few years, implementations of the optical analogue of image scanning microscopy idea by single-point scanning (Heintzmann *et al.*, 2013; Sheppard *et al.*, 2013; Roth *et al.*, 2013) and multipoint scanning (Schulz *et al.*, 2013; Shroff & York 2013; York *et al.*, 2013) were proposed. Our implementation, RCM (De Luca *et al.*, 2013; De Luca, submitted), is a single-point optics-only implementation of the image scanning microscopy idea with two separate pairs of scanning mirrors; the scanner and the re-scanner. With RCM, it is possible to obtain $\sqrt{2}$ improved lateral resolution compared to the diffraction limit. Because RCM uses a sensitive camera for detection, the signal-to-noise ratio in RCM images is improved compared to standard confocal microscopy using photomultiplier tubes for detection.

In addition to the improved resolution and higher sensitivity (De Luca *et al.*, 2013; De Luca, submitted), the RCM has another strong advantage: the optical setup of RCM is flexible in its configuration of excitation lasers, filters and control of the scanning mirrors. This paper shows how RCM can easily be configured to assess biologically driven applications. We show how the super-resolution and the high sensitivity of RCM are also combined with multicolour and high speed imaging. Three configurations were studied in detail: frame-sequential multicolour imaging, line-sequential multicolour imaging and fast single line imaging. Frame sequential multicolour imaging was used to image fixed samples labelled with multiple fluorescent proteins and FRET during HeLa cell apoptosis with the Caspase3-GR sensor. In line sequential multicolour imaging, changes in intracellular calcium concentrations in primary mouse hippocampal neural stem cells and fast ratio-metric measurement of pH in live yeast cells labelled with pHluorin were measured. For fast single line imaging, the speed of subresolution beads in solution and fast fluorescence recovery after photobleaching (FRAP) of mDia2 in HeLa cells was measured. Other configurations will be discussed, but not extensively illustrated with biological applications. All configurations were implemented by exploiting the flexibility of separate control of the scan and re-scan units. The high sensitivity and high resolution of RCM can therefore be combined with this flexible setup and tuned to assess several applications.

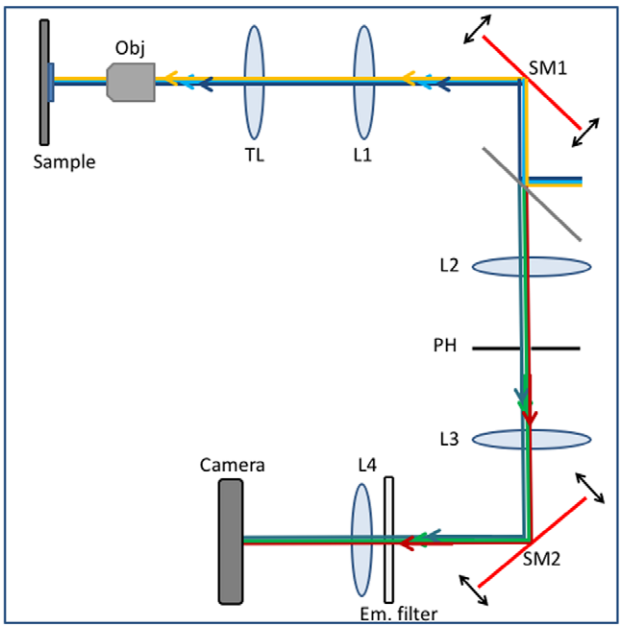


**Fig. 1.** The RCM setup is composed by a standard confocal unit extended via a re-scan unit. The excitation lasers are directed via a dichroic mirror towards the first scanning unit SM1. As in a standard confocal microscope, the scanning unit scans the laser light in the sample and de-scans the emission light, directing it at the pinhole PH. After the pinhole, a second re-scan unit SM2 directs the light onto a camera chip. The resolution of the system can be improved by a factor of $\sqrt{2}$ compared to Abbe's resolution limit. Because of the sensitive camera detection, the SNR of the RCM is four times higher than in standard confocal microscopy. Besides the improved resolution and sensitivity, the RCM optical setup is flexible in its configuration of control of the mirrors, excitation lasers and filters.

### *The basics of the RCM microscope*

RCM is a new super-resolution technique that offers $\sqrt{2}$ higher resolution than Abbe's resolution limit for any pinhole diameter. Furthermore, RCM is equipped with a high-sensitive sCMOS or EMCCD camera as a detector, and therefore has a high sensitivity.

The RCM setup consists of two units: a standard confocal microscope and a re-scan unit (see Fig. 1) (De Luca *et al.*, 2013). In the confocal unit, the scanning mirrors (SM1 in Fig. 1) direct the excitation laser light to the sample and, on the way back, the emission light is directed to the pinhole (de-scanning). After the pinhole, the confocal unit is extended with a re-scan unit including a second pair of scanning mirrors (SM2 in Fig 1). The re-scan mirrors (SM2) direct the emission light that passes the pinhole towards the camera. In the RCM, the presence of two independently controllable scan- and re-scan units, each consisting of a pair of mirrors, a horizontal (x) and a vertical (y) mirror. These four mirrors, here called x-scan, y-scan, x-rescan and y-rescan, are driven from the software. The software driver allows independent adjustment of frequencies ($f_{x,scan}$, $f_{y,scan}$, $f_{x,rescan}$ and $f_{y,rescan}$), amplitudes ($\alpha_{x,scan}$, $\alpha_{y,scan}$, $\alpha_{x,rescan}$ and $\alpha_{y,rescan}$), offset and phase of each

mirrors. For standard RCM imaging, the frequencies of the scan unit and of the re-scan unit are equal. With the angular amplitudes of the mirrors, the magnification can be influenced by adding a mechanical magnification step.

The mechanical magnification in RCM is determined by the angular amplitude $\alpha_{rescan}$ of the re-scan mirrors relative to the amplitude $\alpha_{scan}$ of the scanning mirrors and the focal distances of the scan lenses ($f_1$ and $f_4$). The mechanical magnification is given by:

$$M_{mech} = \frac{f_4 \tan \alpha_{rescan}}{f_1 \tan \alpha_{scan}} \approx \frac{f_4 \, \alpha_{rescan}}{f_1 \, \alpha_{scan}}$$

This approximation is valid because the scan and re-scan angular movement is small (max $\sim 8^{o}$). Together with the magnification $M_{micr}$ of the microscope (combination of tube-lens and objective) the mechanical magnification $M_{mech}$ sets the total magnification $M_{RCM}$ of the RCM system. c

$$M_{RCM} = M_{micr} * M_{mech}$$

In our study, we used a 100x objective ($M_{micr} = 100$).

When the scanning mirrors are set to a fixed position, the magnification will be defined by $M_{micr}$ and an optical magnification $M_{opt}$ determined by the focal distances of the lenses $L_1$, $L_2$, $L_3$ and $L_4$ following:

$$M_{opt} = \frac{f_2}{f_1} * \frac{f_4}{f_3}$$

When the angular amplitudes of scanners and re-scanner are set in such way that $M_{mech} = M_{opt}$, the amplitude of the re-scanner $\alpha_{rescan}$ compensates exactly for the amplitude of the scanner $\alpha_{scan}$. In this specific case, the sweep-factor M, defined by

$$M = \frac{M_{mech}}{M_{opt}}$$

and which expresses the relative mechanical magnification, will equal $M = 1$. The RCM has in this case exactly the same resolution as conventional confocal microscopy.

In general, the total magnification of the RCM microscope can be calculated by $M_{RCM} = M_{micr} * M_{opt} * M$ where the sweep-factor M equals:

$$M = \frac{f_3 \, . \, \alpha_{rescan}}{f_2 \, . \, \alpha_{scan}}$$

The sweep factor M can be adjusted by changing the angular amplitudes of the scanners or by replacing lenses L2 and L3. For $M = 1$, there is no extra magnification due to the sweep factor and the resolution of RCM is the same as for a diffraction limited microscope. For $M = 2$, the spot of emission light projected on the camera chip does not get any larger by this extra magnification because the size of this spot is only determined by $M_{opt}$ and not by $M_{mech}$. Because of the extra re-scan movement, the spot of emission light will be smeared out and the final image will therefore be blurred by a factor of $\sqrt{2}$. Considering the ratio of the two effects (2x extra distance and $\sqrt{2}$ blurring), the result is an image with $\sqrt{2}$ better resolution compared to the diffraction limit.

In conclusion, by re-scanning with double amplitude, a $\sqrt{2}$ resolution improvement can be achieved, without reduction of signal or loss of axial resolution. Since the image is projected directly on the camera chip, RCM does not need any reconstruction software to improve resolution and is therefore fully optical super-resolution technique. Note that this resolution effect is not influenced by the pinhole diameter (De Luca, submitted).

In this paper, the control of the scan and re-scan units, excitation lasers and emission filters of the RCM setup were adjusted to address several biological applications. We show how the pairs of mirrors are controlled not only by adjusting the relative amplitude, but also by adjusting their frequency and phase to tune the microscope, for example, for Forster Resonance Energy Transfer (FRET), calcium activity, ratiometric pH and FRAP measurements.

## Results

### *RCM for frame sequential multicolour imaging*

The optical set-up of a confocal microscope can be configured in several ways in order to record multicolour images. Each configuration has its specific characteristics regarding colour separation. The simplest multicolour configuration is simultaneous scanning where all colours are excited at the same time by one or more lasers, and where the emitted light is separated by dichroic mirrors (either projected on the same camera chip, or split onto separate cameras). Although simultaneous scanning is fast, it has the disadvantage that it is rather costly (if the configuration with multiple cameras is chosen) and that cross-talk between the channels is rather high. Therefore, in this study we did not demonstrate this scanning mode with a biological application.

Sequential scanning, the alternative for simultaneous scanning, is a configuration where the fluorophores are imaged one-by-one. The fluorophores are images sequentially, each excited with a specific wavelength and a specific emission filter. Sequential scanning can be performed line-by-line or frame-by-frame. Frame-by-frame sequential scanning is the simplest configuration to obtain multicolour images with a relatively low crosstalk between the channels. The RCM setup was equipped with three excitation lasers (405 nm, 488 nm and 561 nm), a triple-band dichroic mirror and a filter-wheel with dedicated band-pass filters in front of a single camera. For each fluorophore a separate image was acquired with lasers and emission filters selected accordingly. Obviously, in this configuration there is a time-lag between the images of different colours due to the exposure time for each image plus some extra time for rotation of the emission filter wheel. Therefore, this simple approach is well compatible with the

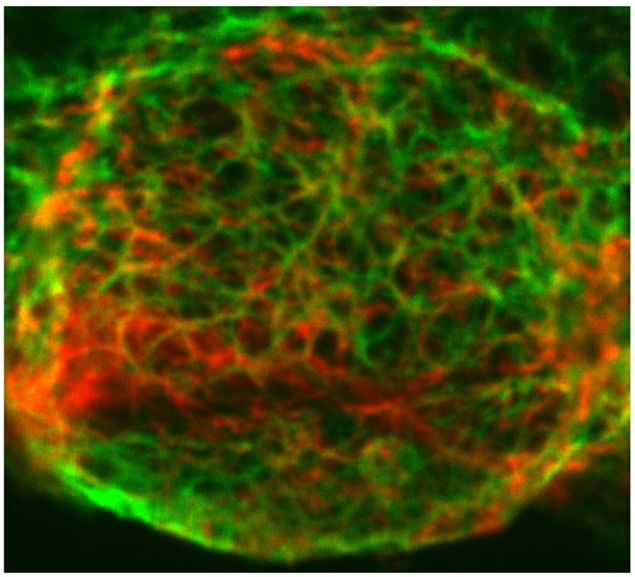

**Fig. 2.** Slice of PA-JEB cell (1 s exposure time) with vimentin and keratin labelled with Alexa 488 and Alexa 555 imaged in RCM multicolour frame-by-frame.

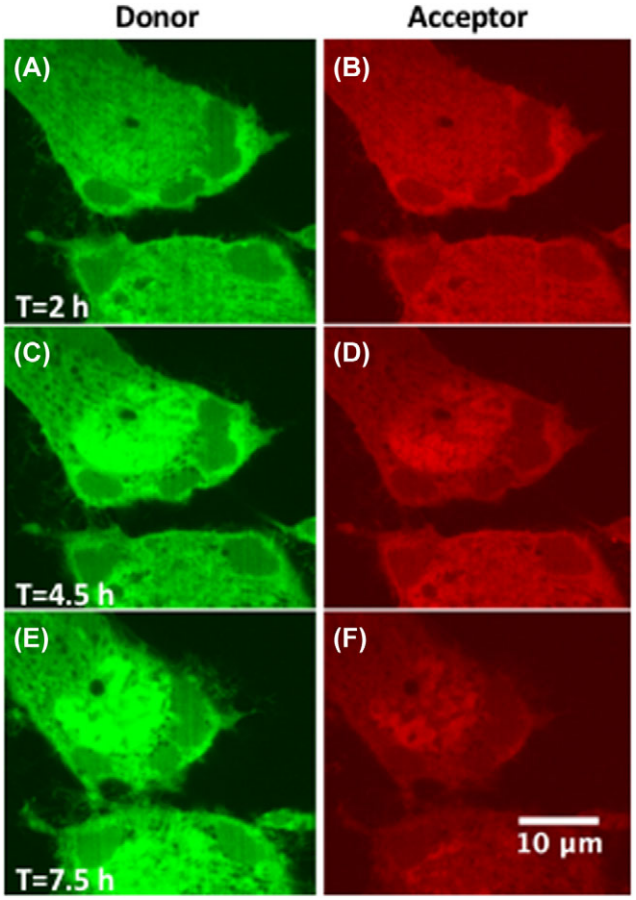


**Fig. 3.** The apoptosis of HeLa cells expressing the TagGFP-TagRFP FRET caspase-3 sensor was imaged in multicolour frame-by-frame RCM imaging. The donor A and the acceptor B channel were imaged at the beginning of the experiment, 2 h after treatment with the apoptosis inducer staurosporine, with initial FRET ratio of $0.68 \pm 0.04$. The two channels were imaged during 5 h of experiment. During apoptosis, the sequence connecting TagGFP and TagRFP cleaves causing a decrease of FRET over time. Therefore, the intensity of the acceptor decreases over time (after 4.5 h, D, and after 7.5 h, F) and the intensity of the donor increases (after 4.5 h, C, and after 7.5 h, E), with final FRET ratio of $0.50 \pm 0.03$.

analysis of fixed multicolour samples, but less suitable for highly dynamic living-cell experiments. To illustrate the applicability of frame sequential multicolour imaging the set-up was used in two biological experiments: dual colour imaging of fixed, double immune stained cells and a live-cell experiment where caspase activity was monitored with a FRET sensor.

For the dual colour imaging of fixed cells, the proteins vimentin and keratin were immuno-labelled in PA-JEB cells with Alexa 488 and 555, respectively (Fig. 2). A 3D-stack was recorded with 200 nm z-step size (one slice is shown in Fig. 2) and the lasers and emission filters were changed for each frame to obtain the dual colour image. Exposure time of each channel per slice was 1 s, and the extra time-lag between the two channels due to filter wheel rotation was 150 ms. Although the disadvantage of the time-lag, this simple method is easy to implement and effective to image fixed samples. The spatial misalignment of the two channels was less than 40 nm (single pixel, measured with 100 nm microbeads, data not shown) and therefore no correction procedure needed to be applied to overlap the green and red image.

In another biological application the frame-sequential multicolour RCM configuration was used to measure FRET in living cell. A FRET-based sensor, caspase3-GR (Shcherbakova *et al.*, 2012), was expressed in order to observe caspase-3 mediated apoptosis in living HeLa cells. The sensor consists of a green (TagGFP) and a red (TagRFP) fluorescent protein connected by a linker containing a caspase-3-specific substrate sequence of amino acids (DEVD). Under standard conditions, the distance between TagGFP and TagRFP molecules is small (relative to the Forster radius) and therefore energy transfer between the molecules, FRET, is efficient. The activation of caspase-3 during apoptosis leads to the cleavage of the DEVD sequence and, therefore the FRET signal between GFP and the RFP is lost (Shcherbakova *et al.*, 2012). Apoptosis was induced by addition of staurosporine to the medium. Two hours after induction of apoptosis, the signal of the donor (TagGFP) and acceptor (TagRFP) was monitored by sequential time-lapse imaging every 10 min (Fig.4) and the ratio of these signals $I_{donor}/I_{acceptor}$ was measured (Jalink & van Rheenen, 2009). At the beginning of the experiment, the donor and the acceptor (Figs. 3A, B) are close enough to allow FRET. The measured FRET ratio $I_{donor}/I_{acceptor}$ was $0.68 \pm 0.04$ (for $t = 2$ h). At $t = 4.5$ h after addition of staurosporine, some cells showed a quick change of the FRET ratio indicating that caspase-3

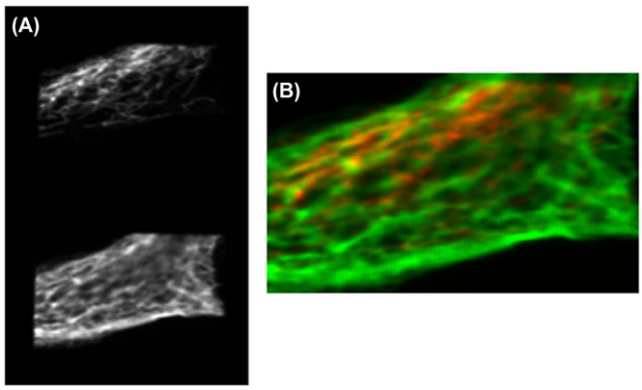


**Fig. 4.** Primary human umbilical vein endothelial cell (HUVECs) were immune-labelled for the vimentin intermediate filaments and Tubulin. The sample was imaged with line-by-line multicolour RCM imaging with 488 nm and 561 nm and the emission multiband filter was a multiband filter (515-550 nm and 600–650 nm band pass). The two colours were projected on the same camera chip (A), the red component on the top and the green component on the bottom part of the chip. The two components have been aligned (B) for the final two-colour image. [Correction added on 6 April 2017, after first online publication: First sentence of figure 4 caption has been corrected]

became active by cleaving the DEVD sequence. Figures 3(C) and (D) clearly show that at 4.5 h after addition of staurosporine the cells were driven into apoptosis. It is possible to notice the decrease of intensity of the acceptor channel and the increase of the intensity of the donor channel due to the reduced FRET between GFP and RFP (Figs. 3C, D). At the end of the imaging experiment (Figs. 3F and G), 7.5 h after staurosporine addition, the apoptosis process was completed for all cells and the FRET ratio was measured to stabilize to a value of $0.50 \pm 0.03$.

These examples show that frame-sequential multicolour imaging can be used for multicolour imaging of fixed cells and FRET analysis of apoptosis in HeLa cells imaged in multicolour with subpixel colour shift.

### *RCM line-by-line multicolour imaging by multiplexing*

For monitoring highly dynamic biological processes, frame sequential scanning for multicolour acquisition is not suitable due to the time-lag between the different colours, during which the sample can change between imaging of the different colours. In standard confocal microscopy this limitation is overcome by line-sequential imaging. Each line of the sample is scanned with two (or more) excitation wavelengths and enabling two (or more) different detectors, each with a fluorophore-specific emission filter. The signals from the detectors are digitized and stored in two (or more) separate images.

In RCM, a similar procedure can be applied. Like in conventional confocal microscopy, line-sequential scanning is also performed by scanning the same line two (or more) times with different fluorophore-specific excitation wavelengths. On the emission side the situation is different; the emitted light is directed to the same camera, but each colour is projected on different areas of the camera chip. In this way the time-lag between the colours is strongly reduced to the order of milliseconds and, consequently, shift between the colours is expected to be negligible. We call this procedure line-by-line sequential multiplexing. Figure 4(A) shows a typical camera image two-colour image by line-sequential multiplexing; The same field of view in different colours is projected on different areas of the camera chip. By a simple affine image transformation (Arganda-Carreras *et al.*, 2006) the two colour components of the image are aligned as shown in Figure 4(B).

Note that the improved lateral resolution (~170 nm), typical for RCM imaging, is also obtained in multicolour imaging by multiplexing. For the choice of emission filter there are three possible configurations: (1) a double band-pass filter and (2) a combination of single band filters, constructed in such way that different parts of the camera chip are covered with different single-band filters. We will call this combined filter the 'church-window' emission filter; (3) it is also possible to use a single band-pass filter, which has specific applications in ratio-metric imaging. For each configuration we will here present a typical biological application.

(1) Double band-pass filter

In the simplest configuration for line-sequential multiplexing a multiband emission filter is used in front of the camera chip. Figure 4(B) shows a fixed PA-JEB human cell immunolabeled for the cytoskeleton proteins vimentin and keratin with Alexa 488 and Alexa 555, respectively. Fluorophores were excited with 488 nm and 561 nm and the emission multiband filter had bands in green (515–550 nm) and red (600–650 nm). The images of the two colour components of the same field of view are projected on the same camera chip (Fig. 4A), the red component on the top and the green component on the bottom part of the chip. The alignment of the two components was performed by calculating the affine transformation between the green and the red channel. The best alignment results were obtained by including translations, scaling, rotation and shear in the transformation matrix (Arganda-Carreras *et al.*, 2006). The transformation was validated by applying the calculated matrix to Tetraspeck bead images (different than the ones used for the transformation calculation) and verifying their re-alignment. After alignment residual colour shift was less than 40 nm (pixel size). The combined image of the double stained PA-JEB cells is shown in Fig. 4B. It is obvious that the maximum field of view is 2 times smaller than the field of view in frame-sequential imaging (Fig. 2). Also the crosstalk between the two channels in this configuration is higher than in frame-sequential scanning since the dual-band emission filter is open for both green and red. For this specific configuration the measured crosstalk was 53±9%, measured

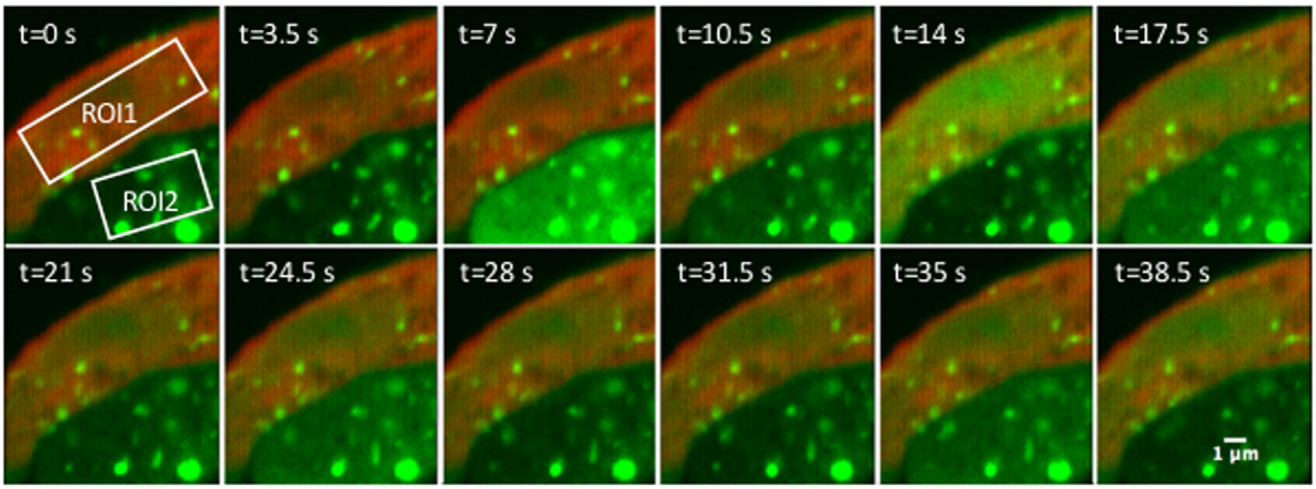


**Fig. 5.** RCM line-by-line multicolour imaging was used with a dedicated 'church-window' emission filter to image spontaneous and histamine-evoked calcium activity in primary mouse neuronal stem cells transfected with AsRed2 and labelled with Fluo4-AM, a green fluorescent calcium-indicator. After stimulation with 100uM histamine, the intensity of Fluo4-AM fluorescence increased up to 25 ± 2% in ROI1 and up to 31 ± 4% in ROI2 after normalization with the intensity of the red channel.

as the ratio of green signal in the red channel (green excitation, red emission) normalized with the value of the red signal. Although the crosstalk is high, the advantage of the line-by-line multicolour imaging is the reduced time-lag between imaging of different colours which is now reduced from several seconds to typically only 2.5 ms. For some biological quantitative measurements, such as FRET measurements and ratio-metric measurements and for very dynamic live-cell imaging, this reduced time-lag can be essential.

(1) 'Church-window' filter

In line-sequential multiplexing the crosstalk between the colour components can be further reduced by using a dedicated filter which has different spectral properties for different areas of the camera chip. The green filter is a 500–550 BP filter and the red filter is a 575 LP filter (Chroma Technology Corp.). Such 'church-window filter' is constructed by assembling the two half mirrors together and positioning them just in front of the camera chip. The crosstalk from green to red was in this specific configuration reduced down to 39 ± 5%. This configuration was tested with imaging of calcium-indicator (Girard & Clapman, 1993) in primary mouse neural stem cells (Fitzsimos *et al.*, 2013) transfected with AsRed2 and labeled with Fluo4-AM, a green fluorescent calcium-indicator. Both spontaneous and histamine-evoked calcium activity was imaged (Fitzsimons *et al.*, 2004), with exposure time of 0.5 s per frame (see Fig. 5). After stimulation with 100 $\mu$M histamine, the intensity of Fluo4-AM fluorescence strongly increased due to increased intracellular calcium concentration. The ratio of red and green intensity was measured and plotted over time, normalized by the intensity of the red channel. The intensity of Fluo4-AM increased up to 25 ± 2% in ROI1 and up to 31 ± 4% in ROI2. This increase shows that hippocampal neural stem cells respond to histamine with changes in intracellular calcium concentrations, confirming previous observations (Tonelli *et al.*, 2012; Apati *et al.*, 2013).

(1) Single band-pass filter

In a third configuration of line-sequential multicolour RCM a single-band filter is used in front of the detector. This configuration was designed for quantitative measurement of intra-cellular pH in living cells as a response to changes of extracellular environmental conditions. The imaging was performed with cells expressing pHluorin in the cytosol. pHluorin is a ratio-metric pH-dependent GFP-derivative (Miesenbock *et al.*, 1998). The protein has an excitation spectrum that changes with the pH of the environment between pH 5.5 and pH 7.5. The emission peak (508 nm) is independent from the pH (Miesenbock *et al.*, 1998). To measure the pH, pHluorin was excited at 405 nm and at 488 nm and imaged by line-sequential multicolour RCM with a single band emission filter (500–550 nm). The ratio between the signal emitted from 405 nm excitation and the signal emitted from 488 nm excitation (405/488 ratio) was measured and later related to the cytosolic pH by means of a calibration curve. This calibration curve was made by measuring the 405/488 ratio in permeabilized cells resuspended in a range of buffers from pH 5 -8 (Fig. 6).

In yeast cells, cytosolic pH is known to respond to glucose availability in the growth media (Orij *et al.*, 2009); During growth, the cytosolic pH is around neutrality but it decreases when glucose is depleted from the media. Glucose re-addition to starved cells triggers a rapid acidification (about 30 s) followed by a recovery of the cytosolic pH to neutral values (Orij *et al.*, 2009). In order to monitor this process with RCM, yeast

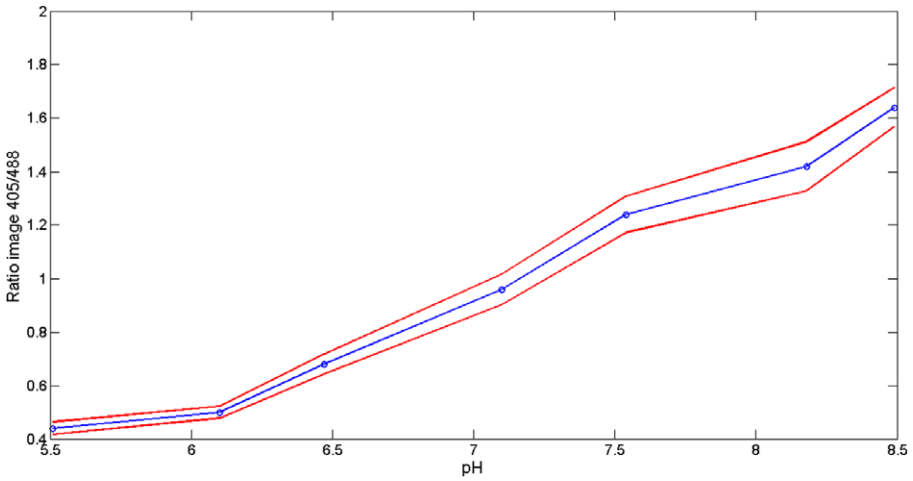


**Fig. 6.** Yeast cells were permeabilized and buffered at different pH in order to calibrate the image ratio $Image_{ratio} = \frac{Image_{405exc}}{Image_{488exc}}$ as a function of the pH of yeast cells. The calibration was used to determine the pH of yeast cells at a measured $Image_{ratio.}$

cells were starved by washing them with culture medium lacking glucose. Starved cells were then imaged and pHc was followed in the RCM upon the addition of glucose to the slide.

The starved yeast cells were imaged during 2 min. At the beginning of the experiment (Fig. 7A), in the absence of glucose, the internal pH was 6.2 ± 0.2. After addition of glucose to the medium, the internal pH increased to 7.6 ± 0.2 (Fig. 7E), which is an average physiological level for yeast cells (Miesenbock *et al.*, 1998). Images representing the pH (Fig. 7 and supplement movie) clearly show a rapid change of pH (~1 min). The alignment of the colour components over time was stable (within the resolution limit) and the system did not need re-alignment during a 1-d experiment. The speed of imaging was limited by the speed of the scanning mirror to 0.5 s per frame for a 50 $\mu m^2$ field of view.

### *RCM fast line scanning*

The speed of imaging in RCM is limited by the speed of the fast scanning and re-scanning mirror (x-direction). In the current set-up the fast mirrors were driven by galvanometers running at a maximum speed of 400 lines per second which limits the frame-rate. Speed can be improved by replacing the galvanometers by resonance scanners. Another option is to give up acquisition of 2-dimensional information and monitor intensity changes along a single line (1-dimensional) at an extremely high imaging rate. By fast scanning over a single line it is possible to obtain intensity information at 400 lines per second, i.e. at time resolution of 2.5 ms. For specific biological applications this single-line configuration can provide specific insight in the dynamic of the specimen as demonstrated in two examples. Here it is shown that this configuration can be used for kymographic detection and analysis of highly dynamic objects and for quantitative measurement dynamics of fluorescent molecules by line-FRAP (van Royen *et al.*, 2009).

For single-line scanning in RCM, the flexibility of the control of the scanning and re-scanning mirrors is exploited. Although the read-out speed of the camera is limited, single-line scanning can be performed by 'writing' a series of lines on the full frame of the camera. In this way the camera image contains now x-versus-time information in contrast with of x-versus-y information in standard microscopy. X-t imaging can be obtained by control of the mirrors in the following way: the x-scan mirror and the x-rescan mirror run synchronously [with the angular amplitude ratio which is typical for RCM ($M = 2$)], the y-scan mirror is static and the y-rescan mirror runs slowly in the t-direction on the camera chip. In this way kymograph imaging was set up.

To demonstrate that single-line scanning can give specific information concerning mobility of particles in solution, a single line across a suspension of 100 nm beads, freely diffusing in water, was imaged with 488 nm excitation beam. The kymographic image (Fig. 8) shows the intensity distribution over a single line (horizontal direction), as a function of time (vertical direction). The line was 25 $\mu$m long and scanned within 1.25 ms. The line frequency was 400 Hz meaning that every 2.5 ms a new line was written. In this experiment 200 lines were written in a full frame in 0.5 s. Fig. 8 show how microbeads, driven by Brownian motion, cross the scanning line indicated by tracks in the x–t space, with the possibility to measure time information from the t-direction, as shown for example in Fig. 8 where a bead was crossing the imaged line in a measured time of 0.07 s. Note that also in this experiment the lateral resolution in the x-direction has the high resolution of RCM. Measured FWHM of the tracks of the 100 nm microbeads (175 ± 11 nm) confirmed the expected high resolution. The kymograph imaging was used to measure the speed of the beads in solution by measuring the length of the track of a single bead in the time-direction. This length, converted to seconds, is a measure of the time in which the

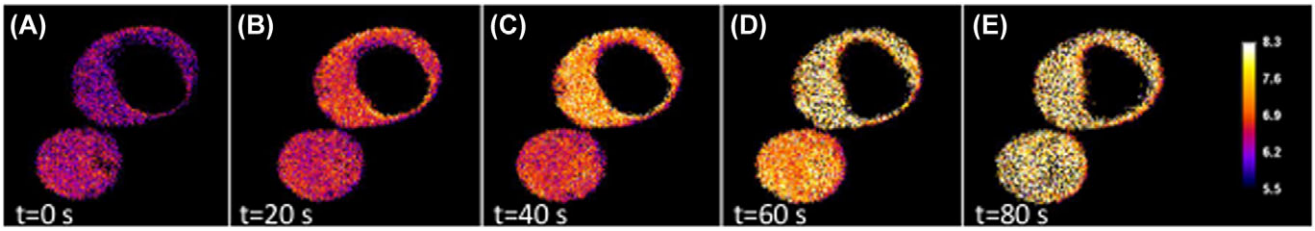


**Fig. 7.** In line-by-line multicolour RCM imaging, starved yeast was imaged immediately prior (A), during (B-D) and after (E) glucose replenishment. The ratio images $Image_{ratio} = \frac{Image_{405exc}}{Image_{488exc}}$ are at 30 s interval. The pH of the yeast cells increases from $6.15 \pm 0.04$ (A) to $7.61 \pm 0.12$ (B) after glucose addition.

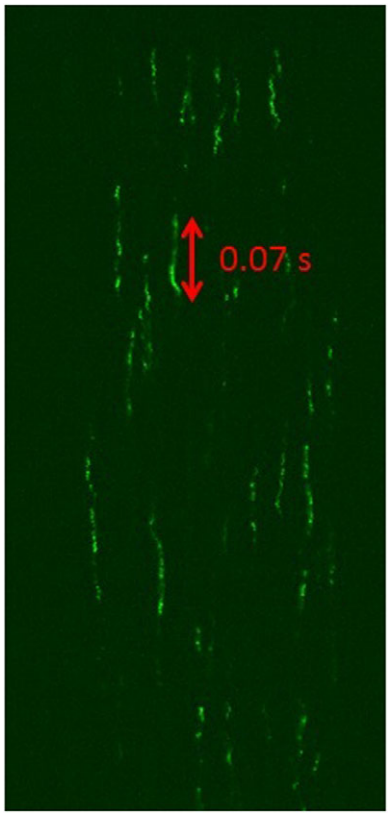


**Fig. 8.** RCM in fast line scanning (kymograph) was used to image beads in solution. A single line in the sample was scanned and the image of the line was re-scanned over time across the camera. The length of the trajectory of a single bead indicates the time in which the bead was passing through the imaged line, for example, 0.07 s for the bead indicated in red in the figure. The kymograph was therefore used to measure the speed of the beads with a measured mean square displacement of $1.7 \pm 0.4\ 10^{-11}$ $m^2\ s^{-1}$.

bead crosses the imaging line. From the average of the length of 100 traces of beads, a mean square displacement of $1.7 \pm 0.4\ 10^{-11}$ $m^2\ s^{-1}$ was measured which is according to measurements reported in literature (Sok Won *et al.*, 2011) based on wide-field microscopy.

In addition to measurement of diffusion of single particles, the single-line scanning configuration can also be used to measure diffusion properties of an ensemble of molecules in a living cell by FRAP. To demonstrate this, the diffusion of the mammalian diaphanous-related formin mDia2 protein was measured in HeLa cells by single-line scanning RCM-FRAP (Fig. 9). The experiment was performed with 488 nm laser excitation and green detection at 2 Hz frame rate and 400 lines per second. A uniform part of the sample of length 5 $\mu$m and width 0.250 $\mu$m (diffraction limited) was imaged in the sample. The FRAP experiment was composed by three imaging periods, all imaged in the same frame. In the first period, the sample was monitored to measure the fluorescence intensity before the bleaching pulse. Then, during a short period, the bleaching pulse was applied and imaged as a bright line. After the bleaching pulse, the recovery was followed over a long period of time. The laser power during bleaching was 250 $\mu$W and after bleaching 10 $\mu$W. The final frame was therefore an image of the same line over time before, during and after line bleaching. For some line-FRAP applications, the information about the spatial distribution of the fluorescence along the imaged line is not necessary. In this case, the fluorescence intensity is integrated along the line and the value of this integral is plotted as a function of time. This mathematical operation can easily be performed in RCM by controlling the scanning and re-scanning mirrors as follows. The fluorescence from the excited line was integrated in a single diffraction-limited spot over time by setting $\alpha_{x,rescan} = 0$ (integrated intensity). By integrating the intensity, the spatial distribution of fluorescence is lost, but the readout of the fluorescence is performed with fewer pixels from the sCMOS camera and therefore thebrk read-out noise decreases. As an example, the FRAP of mDia2 in HeLa cell with integrated intensity is reported in Figure 9(A). The frame, like for the kymograph, includes the imaging of one line in the sample before, during and after bleaching. From the imaging experiments, the characteristic recovery time and the total immobile fractions were estimated by fitting of the FRAP profile. The fluorescence was measured (Fig. 9B) to recover with a recovery half time $\tau_{1/2}$ of $0.07 \pm 0.02$ s and with an immobile fraction of $0.15 \pm 0.03$. The diffusion coefficient of mDia2 was measured $D = 3.2 \times 10^{-12}$ $m^2\ s^{-1}$. This result is in agreement with similar measurement of diffusion coefficient of the same molecule performed in fluorescence correlation spectroscopy (FCS)-FRAP (data not shown) of $D \sim 10^{-12}$. Fast

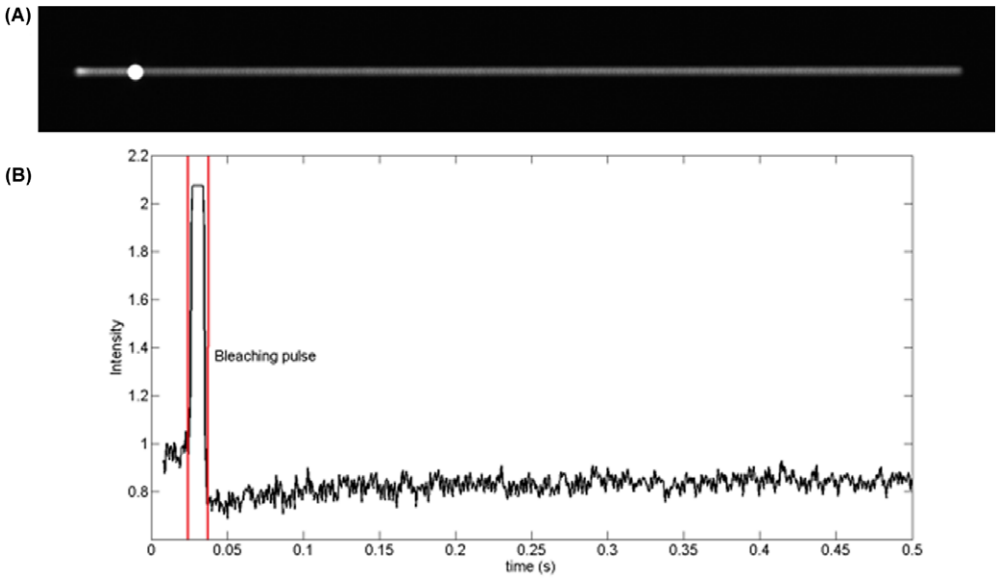


**Fig. 9.** Example of FRAP on mDia in HeLa cells of a single line imaged in fast line scanning (integrated intensity). One line of the sample is imaged and the fluorescence from the line is directed in a single spot on the camera over time. After prebleaching screening, a bleaching pulse was applied and the FRAP recovery is followed over time for a total duration of the experiment of 0.5 s. The intensity across the FRAP curve is plotted in B with a measured diffusion coefficient of $D = 3.2 \times 10^{-12}$ m$^2$ s$^{-1}$.

internal dynamics in line-FRAP were therefore measured with RCM with an imaging speed increased for this application to 400 Hz.

## Conclusions

Because of the independent control of the scan and re-scan units, the RCM can be configured in several ways, each tuned to specific biological questions. These new configurations show how the RCM is potentially flexible for assessing different biological applications. High-resolution multicolour imaging was performed in a frame-by-frame scanning manner and for the first time in a line-by-line scanning manner for calcium activity and ratio-metric pH measurements. Fast single line scanning was performed at high imaging speed for FRAP measurements.

In this paper, only some of the possible configurations of the RCM are shown to illustrate how flexible control of the scanners allows specific configurations. In the future, more settings can be tuned to extend the range of biological applications. For example, the line-by-line multicolour imaging can be performed with more than two colours to monitor fluorescent samples with multiple labelling. Furthermore, the RCM microscope can be configured to do fluorescence correlation spectroscopy measurements by parking the scan mirrors at a fixed position in the sample and let the re-scan mirrors scan across the camera.

So far, the speed of the imaging has been limited by the scanning mirrors. In our setup, the mirrors showed reliable performances until 400 Hz. Further improvement can be achieved by substituting galvo mirrors with the faster resonant mirrors, only if a precise control and synchronization is not a limitation.

The examples reported in this paper show how the potential in fast multicolour live cell imaging of RCM can be exploited not only because of its high resolution and high sensitivity, but also because of the flexible configurations of the mirrors that are only possible with two separate scan and re-scan units. With respect to other implementations of the Sheppard and image scanning microscopy principle (Heintzmann *et al.*, 2013; Roth *et al.*, 2013; Schulz *et al.*, 2013; Sheppard *et al.*, 2013; Shroff & York, 2013; York *et al.*, 2013), RCM is the only setup composed by two different scan and re-scan units that can be controlled independently. This independent mirror control has been exploited in resolution comparison studies (De Luca *et al.*, 2013; De Luca, 2017) with the possibility to change the sweep-factor $M$ from $M = 1$ to $M = 2$ allowing easy resolution comparison. In this paper, we show how this flexibility is necessary to tune the mirrors for expanding the number of biological questions that the RCM can answer, as for example multicolour and single-line imaging. The sensitive camera used in RCM improves the sensitivity of the RCM microscope compared to the confocal microscope (De Luca, 2017), for example, and this improvement might be crucial for longer cell survival in live cell imaging experiments. RCM can therefore be applied in a variety of biological applications and be configured for specific requirements in speed or excitation and emission wavelength and for imaging at high resolution and high sensitivity. This makes RCM a confocal technology with a broad spectrum of applications.

## Materials and method

### *RCM setup*

Light from 405, 488 and 561 nm laser (Melles Griot 405, Obis 488-50, Coherent Inc., Obis 561-20, Coherent Inc.) is coupled into a single mode optical fiber and collimated with a 25 mm lens (ACN127-025-A, Thorlabs Inc.). The light is directed via a 405/488/561/640 nm quad band dichroic mirror (ZT405/488/561/640rpc, Chroma Technology Corp.) to the first xy-scanner (GVSM002/M, Thorlabs Inc.) at the telecentric point of the scan lens of effective focal length 70 mm (CLS-SL, Thorlabs Inc.) and directed to a standard Nikon Ti-E body. The objective in use is 100x Oil 1.49NA Apo-TIRF (Nikon). Fluorescence light is, after de-scanning, focused with a 200 mm achromat (AC254-200-A, Thorlabs Inc.) on a 200 $\mu$m pinhole (Precision Pinholes, Thorlabs Inc.). Light after the pinhole is collected with a 150 mm achromat (AC254-150-A, Thorlabs Inc.) and re-scanned with a second xy-scanner (GVSM002/M, Thorlabs Inc.) and projected with a scan lens of effective focal length 70 mm (CLS-SL, Thorlabs Inc.) on a sCMOS camera (Hamamatsu Flash 4.0) with 2048 $\times$ 2048 pixels of 6.5$\times$6.5 $\mu m^2$. Electronic components of the setup are interfaced by a Nidaq pci-6733 card (National Instruments Co.) via a plug-in in NIS Elements (Nikon Instruments). For line-by-line multicolour imaging mode and fast line scanning, electronic components of the setup are interfaced via LabView.

### *RCM mirrors settings*

Table 1 summarizes the settings of the mirrors that were used for each biological application. The offsets and the phases were equal for all experiments. The offset of the scan unit was set to centre the laser beam at the back aperture of the objective as $\text{offset}_{\text{scan,x}} = 0.5$ V, $\text{offset}_{\text{scan,y}} = -0.7$ V. The offset of the re-scan unit was set to centre the emission light in the centre of the camera chip as $\text{offset}_{\text{rescan,x}} = 1.5$ V, $\text{offset}_{\text{rescan,y}} = 2$ V. The phase of the mirrors where adjusted as $\Delta\varphi = \varphi_{\text{scan,x}} - \varphi_{\text{rescan,x}} = 180^{\text{o}}$ and $\Delta\varphi = \varphi_{\text{scan,x}} - \varphi_{\text{rescan,x}} = 0^{\text{o}}$.

### *Overlapping of line-by-line multicolour RCM images*

After imaging with the RCM multicolour settings, the acquired image shows the same field of view from different excitation lines one on top of the other. It is therefore necessary to crop the two fields of view and align them one on top of each other. The calibration elastic transformation was first calculated with Tetraspeck beads (Invitrogen) by the ImageJ plugin bUnwarpJ. The calculated transformation from the calibration beads was then applied to the acquired images.

The calibration images used to calculate the transformation matrix where acquired by imaging Tetraspeck beads (Invitrogen). The beads were excited with 405 nm and 488 nm lasers and the emission detected with a multiband filter (450-470/515-550/600-650 BP). The image of the same field of beads excited at 405 and 488 nm was acquired at 1 s exposure time. The elastic transformation has been calculated by the ImageJ plugin bUnwarpJ (Arganda-Carreras *et al.*, 2006), that calculates elastic deformations represented by B-splines between two 2D images. The two images of the beads at different colours are respectively selected as 'source' and 'target' for the algorithm and the transformation matrix between source and target is calculated. For what concerns the parameters for the alignment, the Registration Mode was set 'accurate', the Initial Deformation 'very coarse' and the Final Deformation 'very fine'. No landmarks were set to calculate the transformation to prevent possible user's errors. The algorithm saves the direct and inverse transformations into files.

After calculating the transformations with the bead images, the calculated transformations were applied to the yeast images of the same field of view acquired with the same mirrors settings. The background determined from dark images (laser off, same exposure time as the standard imaging conditions) was subtracted to the final aligned images and the ratio image $Image_{ratio}$ was calculated as $Image_{ratio} = \frac{Image_{405exc}}{Image_{488exc}}$.

### *Cross-talk measurement*

The cross-talk was measured with FluoCells Prepared Slide #6 (Muntjac cells with Mouse Anti-OxPhos Complex V Inhibitor Protein, Alexa Fluor® 555 Goat Anti-Mouse IgG, Alexa Fluor® 488 Phalloidin, and TO-PRO®-3, Thermofisher Inc.). The sample was imaged with 488 nm excitation laser light and red detection (575 LP) to obtain the cross-talk image. The cross-talk image was normalized by the standard red image (561 nm excitation laser light, 575 LP detection).

### *PA-JEB and HUVEC sample preparation*

Pyloric atresia junctional epidermolysis bullosa (PA-JEB) keratinocyte cells expressing $\beta$4 integrin (PA-JEB/$\beta$4) were cultured as described previously (Geerts *et al.*, 1999). For immunofluorescent analysis, keratinocytes grown on cover slips were fixed with 10% MeS buffer (100 mM MeS, pH 6.9, 1 mM EGTA and 1 mM MgCl2) and 90% methanol for 5 min on ice. After blocking with 5% bovine serum albumin for 1 hour, the cells were incubated with mouse anti-vimentin monoclonal antibody (Clone V9-Dako) and rabbit anti-keratin 14 polyclonal antibody (Covance) for 1 hour. Subsequently all the cells were incubated with goat anti-rabbit and goat anti-mouse antibodies (Alexa 488 and Alexa 555 Invitrogen) for 30 min. All the fixation and staining steps were done at room temperature. Primary human umbilical vein endothelial cells (HUVECs) were cultured, fixed and stained as described before (Nieuwenhuizen *et al.*, 2015; Nahidiazar *et al.*, 2015).

[Correction added on 6 April 2017, after first online publication: heading "*PA-JEB sample preparation*" has been corrected and an extra sentence added at the end of paragraph]

**Table 1.** Settings of the mirrors for the different biological application of RCM described.

| Configuration | Appl. | $V_{scan,x}$ | $V_{scan,y}$ | $V_{rescan,x}$ | $V_{rescan,y}$ | $f_{scan,x}$ | $f_{scan,y}$ | $f_{rescan,x}$ | $f_{rescan,y}$ |
|---|---|---|---|---|---|---|---|---|---|
| Frame sequential multicolour imaging | FRET | 2 V | 3 V | 2.08 V | 5.28 V | 400 Hz | 1 Hz | 400 Hz | 1 Hz |
| Line-by-line multicolour imaging | pH | 0.7 V | 0.65 V | 1.46 V | 1.14 V | 400 Hz | 1 Hz | 200 Hz | 1 Hz |
| Fast line scanning (kymograph) | Beads | 2 | 0 | 2.08 V | 4.5 V | 400 Hz | 0 | 400 Hz | 2 Hz |
| Fast line scanning (integrated intensity) | FRAP | 2 | 0 | 0 | 4.5 V | 400 Hz | 0 | 0 | 2 Hz |

*FRET Sample preparation*

Plasmids have been prepared using a mini prep kit (Thermo Scientific) as in (Shcherbakova *et al.*, 2012). The plasmids contain the sequences for the TagGFP and the TagRFP, separated by the caspase-3 cleavage sequence, DEVD.

HeLa cells were seeded on 25 mm glass cover slips in a 6-well plate and cultured in optim MEM medium supplemented with 10 % FBS (Invitrogen) and 0,5% penicillin-streptomycin (Invitrogen). Transfections were performed with the plasmids described above using PEI as transfection reagent and imaged after 2 days after transfection.

For sample preparation, a glass cover slip from the 6-well plate was placed in a cell chamber with 500 $\mu$l of microscopy medium. The cells were then treated with 2 $\mu$M Staurosporine (LC Laboratories) prior the start of the experiment.

*NSPC sample preparation*

Mouse hippocampal NSPCs were cultured as described before (PMID: 26207921, PMID: 22925833). 2 days prior to imaging, $2.5\times10^5$ cells were seeded on laminin/PLA-coated 35mm cover slips. To fluorescently label the NSPCs, one day after seeding AsRed2 plasmid (2500 ng/cover slip) was transfected into the NSPCs using Attractene transfection reagent (Qiagen) following manufacturer's instructions, as described before (PMID: 26207921). On the day of imaging, NSPCs were loaded with Fluo4-AM (ThermoFIsher Scientific), a green fluorescent calcium indicator following manufacturer's instructions. To prevent Fluo4-AM leakage from the cells, the organic anion-transport inhibitor Probenecid (thermoFisher Scientific) was added to the loading solution. Loading solution consisted of 1:1000 Fluo4-AM, 1:100 Probenecid, and 1:100 Powerload (ThermoFisher Scientific). NSPCs were incubated with loading solution for 30 min at 37°C, followed by 30 min at room temperature. After loading, cells were washed once with culture medium before proceeding to imaging. Evoked calcium-activity was imaged using 100 $\mu$M histamine in culture medium.

*Yeast sample preparation*

The yeast used for this study is from the haploid strain BY4741 with genotype MATa, his3D1, leu2D0, met15D0, ura3D0. The cells are kept and grown in a media including the nutrients, except the amino acids used to add the plasmids. The media used for this study is a Synthetic Complete (SC) media. The yeast was imaged with an Optical Density (OD) between 5 and 10, ensuring the best conditions for cells viability. The cells are kept in a saturated culture at cold temperature.

For the calibration curve, cells expressing pHluorin were imaged in buffers of defined pH: a set of buffers is prepared mixing 0.1 M citric acid and 0.2 M $Na_2HPO_4$ in different relative quantities to cover a buffer range from pH 5.5 to pH 8.5. The yeasts are grown overnight in 20 mL media to a concentration of 10 OD. They are permeabilized with 100 $\mu$g mL$^{-1}$ digitonin in PBS for 10 min. The digitonin creates pores in the cell membrane; in this case, the extracellular pH is the same as the intracellular pH. The cells are washed and concentrated in PBS in Eppendorf tubes.

For yeast imaging at physiological pH, yeasts expressing pHluorin are grown overnight in 10 mL media to a concentration of 10 OD. The starvation is obtained by isolating yeast cells at physiological conditions from their culture medium and substituting it with glucose-free medium. The imaging was performed after 1 h from the isolation. For the sample imaging preparation, 7 $\mu$L of yeast solution is pipetted on an Nr.1 cover slip (Menzel-Glaser) and a layer of Agarose is positioned on top of the cells to fix them to the cover slip. For the pH calibration curves, the cover slips were subsequently mounted on a microscope coverglass (Menzel-Glaser). For the glucose addition experiments, the cover slips were subsequently mounted on a microscopy imaging ring.

*Beads sample preparation*

Hundred nanometres diameter yellow-green fluorescent beads (Invitrogen) were diluted at $10^{-6}$ M solution. 0.5 mL of beads solution and 0.5 mL of distilled water where mixed and 0.15 mL of the final solution was mounted on a Nr.1 cover slip (Menzel-Glaser) and on an imaging ring.

**Acknowledgements**

The authors thank T. W. J. Gadella, M. A. Hink and P.A.C. Joosen for the useful discussions about the biological applications and the FRET and FRAP sample preparation. The authors thank B. van der Broek for the ImageJ alignment plugin. The authors thank P. Drent (Confocal.nl BV) for arranging the 'church window' filter assembly, G. J. Brakenhoff for the useful discussions, ideas and support, M. Schouten for providing the

neural stem cells. The authors thank Prof. Arnoud Sonnenberg for the PAJEB cells. The authors thank Prof. Kees Jalink for discussions and applications. This research is financially supported by the Dutch Technology Foundation STW. G.M.R.D.L. is supported by the Dutch Technology Foundation STW project 11350. P.B. and C.P.F. are funded by the Netherlands Organization for Scientific Research (NWO Vidi H64.09.016) and Internationale stichting Alzheimer onderzoek (ISAO).

## References

Apati, A., Paszty, K., Hegedus, L., *et al.* (2013) Characterization of calcium signals in human embryonic stem cells and in their differentiated offspring by a stably integrated calcium indicator protein. *Cell Signal.* **25**(4), 752–759.

Arganda-Carreras, I., Sorzano, C.O.S., Marabini, R., Carazo, J.M., Ortiz-de Solorzano, C. & Kybic, J. (2006) Consistent and elastic registration of histological sections using vector-spline regularization. *Lecture Notes in Computer Science, Springer, 4241/2006, Computer Vision Approaches to Medical Image Analysis*. pp. 85–95. Springer.

Betzig, E., *et al.* (2006) Imaging intracellular fluorescent proteins at nanometer resolution. *Science*. **313**(5793), 1642–1645.

De Luca, G.M.R., Breedijk, R.M.P., Manders, E.M.M., *et al.* (2013) Re-scan confocal microscopy: scanning twice for better resolution. *Biomed. Opt. Exp.* **4**, 2644–2656.

De Luca, G.M.R., Breedijk, R.M.P., Manders, E.M.M., *et al.* (2017) Re-scan Confocal Microscopy (RCM) improves the resolution of confocal microscopy at increased sensitivity, *Methods and Applications in Fluorescence*.

Fitzsimos, C.P., van Hooijdonk, L.W., Schouten, M., *et al.* (2013) Knochdown of the glucocorticoid receptor alters functional integration of newborn neurons in the adult hippocampus and impairs fear-motivated behavior. *Mol. Psychiatry*. **18**(9), 993–1005.

Fitzsimons, C.P., Monczor, F., Fernandez, N., *et al.* (2004) Mepyramine, a histamine H1 receptor inverse agonist, binds preferentially to a G protein-coupled form of the receptor and sequesters G protein. *J. Biol. Chem*. **279**(33), 34431–34439.

Geerts, D., Fontao, L., Nievers, M.G., *et al.* (1999) Binding of integrin alpha6beta4 to plectin prevents plectin association with F-actin but does not interfere with intermediate filament binding. *J. Cell Biol*. **147**, 417–434.

Girard, S. & Clapman, D. (1993) Acceleration of intracellular calcium waves in Xenopus oocytes by calcium influx. *Science*. **260**(5105), 229–232.

Heintzmann, R., Roth, S., Sheppard, C., *et al.* (2013) Verfahren zum optisch hochaufgelösten Rasterscanning eines Objekts. *Patent Publication Number DE* 102013005927 A1.

Hess, S., Giririjan, T. & Mason, M. (2006) Ultra-high resolution imaging by fluorescence. *Biophys. J*. **91**(11), 4258–4272.

Jalink, K. & van Rheenen, J. (2009) FilterFRET: quantitative imaging of sensitized emission. *FRET and FLIM Techniques, Laboratory Techniques in Biochemistry and Molecular Biology* (ed. by T.W.J. Gadella), Vol. **33**, pp. 289–349. Elsevier.

Leung, B.O. & Keng, C.C. (2011) Review of super-resolution fluorescence microscopy for biology. *Appl. Spectrosc*. **65**(9), 967–980.

Marx, V. (2013) Is super resolution microscopy right for you? *Nat. Methods*. **10**, 1157–1163.

Miesenbock, G., De Angelis, D.A. & Rothman, J.E. (1998) Visualizing secretion and synaptic transmission with pH-sensitive green fluorescent proteins. *Nature*. **394**, 192–195.

Muller, C.B. & Enderlein, J. (2010) Image scanning microscopy. *Phys. Rev. Lett*. **104**, 198101-1:198101-4.

Nahidiazar, L., Kreft, M., van den Broek, B., Secades, P., Manders, E.M.M., Sonnenberg, A., *et al.* (2015) The molecular architecture of hemidesmosomes, as revealed with superresolution microscopy. *J. Cell. Sci.* **128**, 3714–3719.

Nieuwenhuizen, R.P.J., Nahidiazar, L., Manders, E.M.M., Jalink, K., Stallinga, S., & Rieger, B. (2015) Co-Orientation: quantifying simultaneous co-localization and orientational alignment of filaments in light microscopy. *PLoS ONE*. **10**(7), 0131756-1–0131756-21.

Orij, R., Postmus, J., Ter Beek, A., Brul, S. & Smits, G.J. (2009) In vivo measurement of cytosolic and mitochondrial pH using a pH-sensitive GFP derivative in Saccharomyces cerevisiae reveals a relation between intracellular pH and growth. *Microbiology*. **155**, 268–278.

Roth, S., Sheppard, C.J.R., Wicker, K. & Heintzmann, R. (2013) Optical photon reassignment microscopy (OPRA). *Opt. Nanosc*. **2**, 2192–2853.

Rust, M., Bates, M. & Zhuang, X. (2006) Sub-diffraction-limit imaging by stochastic optical reconstruction microscopy (STORM). *Nat. Methods*. **3**(10), 793–796.

Schermelleh, L., Heintzmann, R. & Leonhardt, H. (2010) A guide to super-resolution fluorescence microscopy. *J. Cell Biol.* **190**(2), 165–175.

Schulz, O., Pieper, C., Clever, M., *et al.* (2013) Resolution doubling in fluorescence microscopy with confocal spinning-disk image scanning microscopy. *PNAS*. **10**(52), 21000–21005.

Shcherbakova, D.V., Hink, M.A., Joosen, L., Gadella, T.W.J. & Verkhusha, V.V. (2012) An orange fluorescent protein with a large Stokes shift for single-excitation multicolor FCCS and FRET imaging. *J. Am. Chem. Soc*. **134**, 7913–7923.

Sheppard, C.J.R. (1988) Super-resolution in confocal imaging. *Optik*. **80**, 53–54.

Sheppard, C.J.R., Mehta, S.B. & Heintzmann, R. (2013) Superresolution by image scanning microscopy using pixel reassignment. *Opt. Lett.* **38**, 2889–2895.

Shroff, H. & York, G. (2013) Multi-focal structured illumination microscopy and methods. *Patent Publication Number* WO2013/126762 A1

Sok Won, K., Yesul, H. & Lee, J. (2011) Measurement of diffusion coefficients of fluorescence beads and quantum dots using fluorescence correlation spectroscopy. *J. Korean Phys. Soc*. **59**(51), 3177.

Tonelli, F.M., Santos, A.K., Gomes, D.A., *et al.* (2012) Stem cells and calcium signaling. *Adv. Exp. Med. Biol*. **740**, 891–916.

van Royen, M.E., Dinant, C., Farla, P., *et al.* (2009) FRAP and FRET methods to study nuclear receptors in living cells. *Meth. Mol. Bio*. **505**, 69–96.

York, A.G., Chandris, P., Shroff, H., *et al.* (2013) Instant super-resolution imaging in live cells and embryos via analog image processing. *Nat. Meth.* **10**, 1122–1126.

[Correction added on 6 April 2017, after first online publication: Acknowledgement to two professors and two new references have been added]